Source location and wavefield characterization of river-induced seismic tremor- A case study near Avoca River, Ireland

Haleh Karbala Ali[1] and Christopher J. Bean[2]
[1]Postdoc Researcher, Geophysics Section, School of Cosmic Physics, Dublin Institute for Advanced Studies (DIAS), Dublin, Ireland, haleh@cp.dias.ie
[2]Geophysics Section, School of Cosmic Physics, Dublin Institute for Advanced Studies (DIAS), Dublin, Ireland ,chris.bean@dias.ie

Key Points:

- Locating the river-induced seismic signal (tremor) using beamforming array analysis
- Characterization of the tremor wave components using Frequency Dependent Polarization Analysis (FDPA),
- Correlation of the tremor with flow-rate as an indirect monitoring tool.

Key Words:

River-induced seismic tremor, Source location, Beamforming array analysis, Frequency dependent polarization analysis, Wavefield monitoring,

Abstract

Turbulency of water flow and sediments carried in water courses are the main causes that induce tiny ground vibrations which cannot be sensed by humans even if standing close to the river. This micro vibrations can however be detected and monitored by sensitive seismic instruments placed adjacent to the river . Detection of this ground vibrations becomes challenging when the river is near a construction site, railway, local roads, and residential areas as human activities also shake

the ground. This study shows that we can infer the change in river flow-rate based on how strong the earth is shaking on different days of data recording.

1 Introduction

Different hydraulic processes in surface rivers induce ground vibrations in the range of nano- to micro-meters that can be identified by deploying sensitive seismic stations in close proximity to the river. These processes include turbulent water flow, bed-load transport, air bubbles explosion, and generation of gravity or breaking waves at the river surface (Schmandt et al., 2013, Laros et al., 2015). Govi et al. (1993) were the first to report the change in seismic signal amplitude due to variation in discharge conditions. Huang et al. (2007) explored the origins of ground vibrations caused by debris flows. Burtin et al. (2008, 2011) explored the use of seismic noise produced by rivers to monitor the bed load transport for the trans-Himalayan Trisuli river and the low-discharge Torrent de Saint Pierre braided river in the French Alps, respectively. Burtin et al. (2010) located the Trisuli river-induced seismic signal using noise correlation functions. Winberry et al. (2009) reported the resonance of subglacial cracks and conduits containing water as a sustained seismic tremor and could track and locate the tremor using array analysis. Tsai et al. (2012) developed the first forward model describing the power spectral density of Rayleigh waves generated through the impacts of grains on the river bed. Gimbert et al. (2014) introduced a mechanistic model describing seismic signal generation as a result of time-varying normal and shear stress of turbulent water- flow against the river bed. Gestrich et al. (2020) developed a physical model for volcanic eruption tremor based on similarities in physical processes and observed seismic tremor in rivers. Bartholomaus et al. (2015) quantified the seasonal subglacial discharge based on the tremor power. Schmandt et al. (2017) used a dense array along Trinity River in a dam-controlled and gravel augmentation experiment to study the spatio-temporal extent of sediment transport. Anthoney et al. (2018) observed a low-frequency signal sensitive to discharge dominant on horizontal components of stations within 1 m of the channel boundary as a result of sensor tilt due to viscoelastic deformation in the hyporheic zone. Goodling et al. (2018) studied dam spillway monitoring based on Frequency-Dependent Polarization Analysis (FDPA) to locate the turbulence flow and characterize the surface waves induced by dam floods. Vore et al. (2019) studied the subglacial water systems using FDPA to distinguish between single and multi-conduit flow paths and characterization of the seismic tremor. Coviello et al. (2019) proposed a debris flow detection algorithm based on the amplitude information gathered from a linear array of geophones installed along the channel in an early warning system. Eibl et al. (2020) located and tracked the subglacial flood front based on array analysis of the seismic tremor and reported early warning capability. To our knowledge, the study we report herein combines, for the first time, the application of array processing using clusters of seismic stations (arrays) and Frequency-Dependent Polarization Analysis (FDPA) based on single three-component seismic stations to locate river-induced seismic tremor and characterize tremor wave-type composition. Here we observed different wave components within river-induced tremor and showed that Love waves are more prevalent than Rayleigh waves. We interpret this as indicative of strong coupling at the river bed. We also observed the enhancement in Rayleigh wave composition after 5:00 A.M. which can be attributed to noise induced by daily cultural activities trapped in the river. Finally, the correlation observed between flow-rate and river-induced tremor, despite the extensive amount of cultural noise at our site, confirmed the applicability of fluvial seismology for monitoring rivers even in urban settings and areas with strong cultural noise.

2 Methods

2.1 Research Site and Instrumentation

We conducted the experiment between 10th-15th October 2019 next to Avoca River, County Wicklow, Ireland. The main reason for choosing this site for the experiment was the existence of permanent monitoring flow-gauges belonging to the Environmental Protection Agency (EPA). This enabled us to investigate the correlation between water-level/flow-rate change, with changes in seismic signature induced by the river. The study site located close to Wicklow County Council construction site, a railway line, and local road, therefore the data were highly contaminated by cultural noise, which in its serves as an interesting case study. We used three-components (3C) Lennartz short-period 1Hz seismometers and data-cube digitizers with a sampling frequency of 200 Hz. We deployed stations AV001- AV013 on October 10th and stations AV014- AV017 on October 14th and retrieved them on October 15th 2019. We deployed two seismic arrays, up-and down-stream of the river, each consisting of 6 and 4 stations, respectively. When a cluster of seismic stations is deployed together they constitute a seismic array. With an array we can locte the azimuth from which the microtremor is coming, and also calculate its apparent velocity, which holds information about the seismic wave-type composition of the tremor. We deployed station AV009 close to the river where the flow gauge was mounted to investigate the correlation between flow-rate/water-level data from the flow gauge and the river-induced seismic signal, until December 18th 2019. Figure 1 shows the location map of the Avoca River, the deployed seismic stations and arrays, and the EPA flow gauges. To alleviate the effect of noise on seismic data we buried all seismic sensors in 30cm-deep pits. Figure 2 shows the seismometer, data-logger, and deployment in the field.

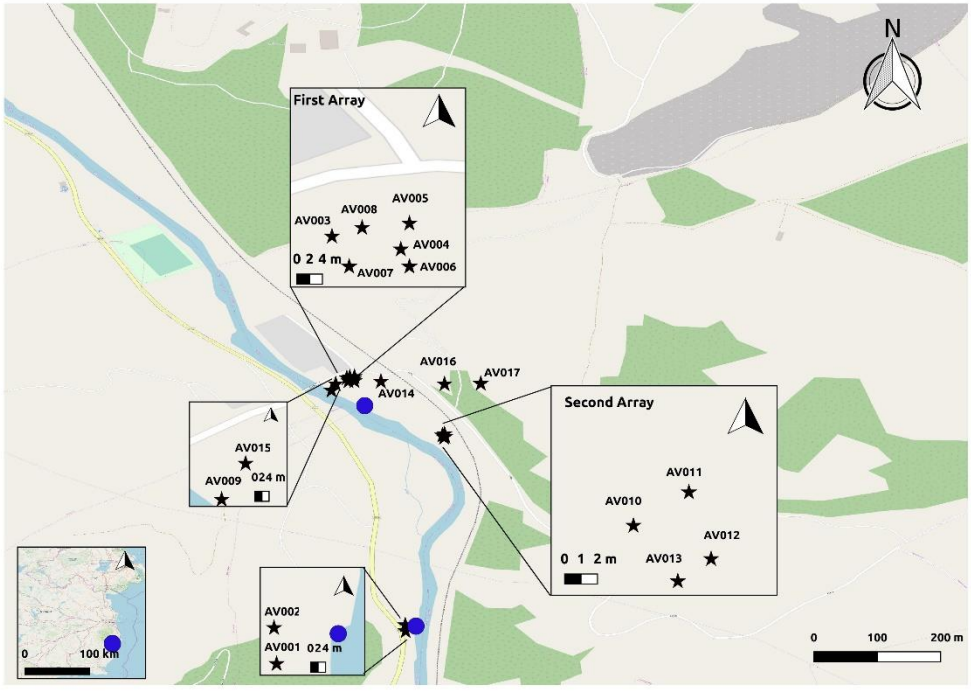

Figure 1. The location map of the experiment next to the Avoca River, County Wicklow, Ireland between 10th- 15th October 2019. The deployed seismic stations and the EPA flow-gauges are

shown as stars and blue circles, respectively.

Figure 2. Seismic instruments used throughout the fieldwork. (a) Three-component (3C) Lennartz short-period 1Hz seismometer, data-cube digitizer and breakout-box to connect the seismometer tothe data-logger, (b) deployment of a seismometer in a 30cm deep pit to alleviate the effect of cultural, wind and rain noise.

2.2 Beamforming Array-processing

The river-induced seismic tremor has no definite onset, so we cannot use the conventional earthquake location methods based on P- and S-wave arrivals to determine the direction of arrival of the seismic signals. However, by deploying a group of stations as an array, we could apply frequency-wavenumber (F-K) analysis to simultaneously determine the back-azimuth (BAZ), i.e., the direction of arrival of the wavefront measured with respect to the North, and the apparent slowness, i.e., the inverse of apparent wave speed. For the joint determination of back-azimuth and apparent slowness of a wave, both frequency-domain methods and time-domain methods exist. Here, we performed a frequency wavenumber (FK) analysis with a moving time window. The FK analysis is a beamforming method in the spectral domain that performs a grid search within a horizontal slowness grid (s_x and s_y). In each time window, the covariances of the Fourier Transformed signal at each receiver pair are calculated. Phase delays of each plane wave described by the horizontal slowness grid are applied and the trace of the resulting covariance matrix is the cross-spectral density. This is undertaken for every grid point and results in absolute power and semblance maps (ratio of the averaged power of the stacked trace and the stack of the average single trace powers) in the spectral domain with respect to the horizontal slownesses. The maximum value in these maps is determined and converted to back-azimuth and slowness of the incoming wave using the angle and length of the vector from the origin to the maximum, respectively. The underlying assumptions include a plane wavefront, coherent signal and incoherent noise (Eibl et al., 2017). The array processing output is a time-series of BAZ, apparent slowness, absolute and relative power (semblance). The dominant BAZ for each array is the maximum of BAZ histogram and the dominant slowness value is the median of the slowness time-series.

2.3 Frequency-Dependent Polarization Analysis

Frequency-Dependent Polarization Analysis (FDPA) originally introduced by Park (1987) can be used to determine different wave components such as Rayleigh, Love and body waves in the tremor and determine the BAZ of the arriving waves when Rayleigh waves dominate. In this study, we

applied the method described by Vore et al. (2019). For the 3C seismic data at each station, we divided the signal into 60-second-long windows with a 50% overlap. After applying the Fourier Transform to each component, the covariance spectral matrix for each frequency component is calculated. An average spectral covariance matrix is then computed by linearly averaging the real and imaginary parts of 7-minute binned data to eliminate short-transients. The polarization vector can be defined when the ground motion is mostly constrained within a single plane of motion when the first singular value of the average spectral covariance matrix is larger than the other two. We set the threshold value to 2. The wave composition of the tremor can be identified based on the phase-lag between the vertical and horizontal components. If phase-lag is between 0-20 degrees, either body or Love waves dominate the tremor with linear particle motion, whereas Rayleigh waves having elliptical particle motion exhibit phase-lag between 70-90 degrees. Further differentiation between Love and body waves is possible by comparing the power spectra of the vertical and horizontal components at each frequency. If the magnitude of the horizontal power (average of the two horizontal components) is higher than the vertical one, the signal is Love-wave dominated otherwise it consists mainly of body waves. The percentage of different wave types for each frequency component is determined by choosing a 20% threshold. When Rayleigh waves dominate, it is possible to determine the BAZ based on the amplitude ratio between horizontal components of the polarization vector.

3 Data

All the stations successfully recorded data for the whole deployment period. We removed the linear trend from the data, tapered, and corrected for the instrument response. We applied a low-cut filter to remove microseism (signals induced by ocean processes) which appeared quite strong in the low-frequency range below 3 Hz on our dataset. As the river produces a continuous seismic source in time, the river-induced signal appears as a persistent frequency band on spectrograms. In the following, we refer to the river-induced seismic signal as the tremor. We computed the spectrograms of different stations with 8-second sliding windows of 50% overlap. Figure 3 shows the spectrogram of the stations AV002, AV009, AV003, and AV011 on October 15th, 2019 from midnight to 08:30 A.M. We deployed stations AV002 and AV009 very close to the river (<10m). Note the Station AV003 belongs to the first seismic array deployed upstream 50m from the river and station AV011 is a representative station from the second array deployed downstream 30m from the river. We noticed the shift of the tremor persistent frequency band on spectrograms depending on the seismic station offset to the river. The high frequencies get attenuated with distance from the river as shown in the spectrogram of station AV003. Some background cultural noise appears as vertical spikes on the spectrograms. Note the cultural noise enhances from 5:00 A.M. which is the start of daily human activities. The narrow-band signal at 50 Hz is induced by the electric power cables near the stations. The narrow band signals at 40 and 60 Hz are also stationary noise.

4 Results

Here we show the results of applying beamforming on October 15th, 2019 from midnight to 08:30 A.M. for the first and second arrays. We bandpass filtered the seismic data in the discrete persistent frequency bands observed on the spectrograms of the first array including 8-10, 10-14.26, and 19-22 Hz. The data set is divided into 60-second-long time-windows with 50% overlap. In each of these windows, the standard FK analysis is performed. The result is a time series of BAZ, horizontal slowness and relative power (semblance) of the predominant signal in each time

window. Changes in the BAZ suggest a source movement, while a change in slowness reveals different seismic wave types arriving at the array.

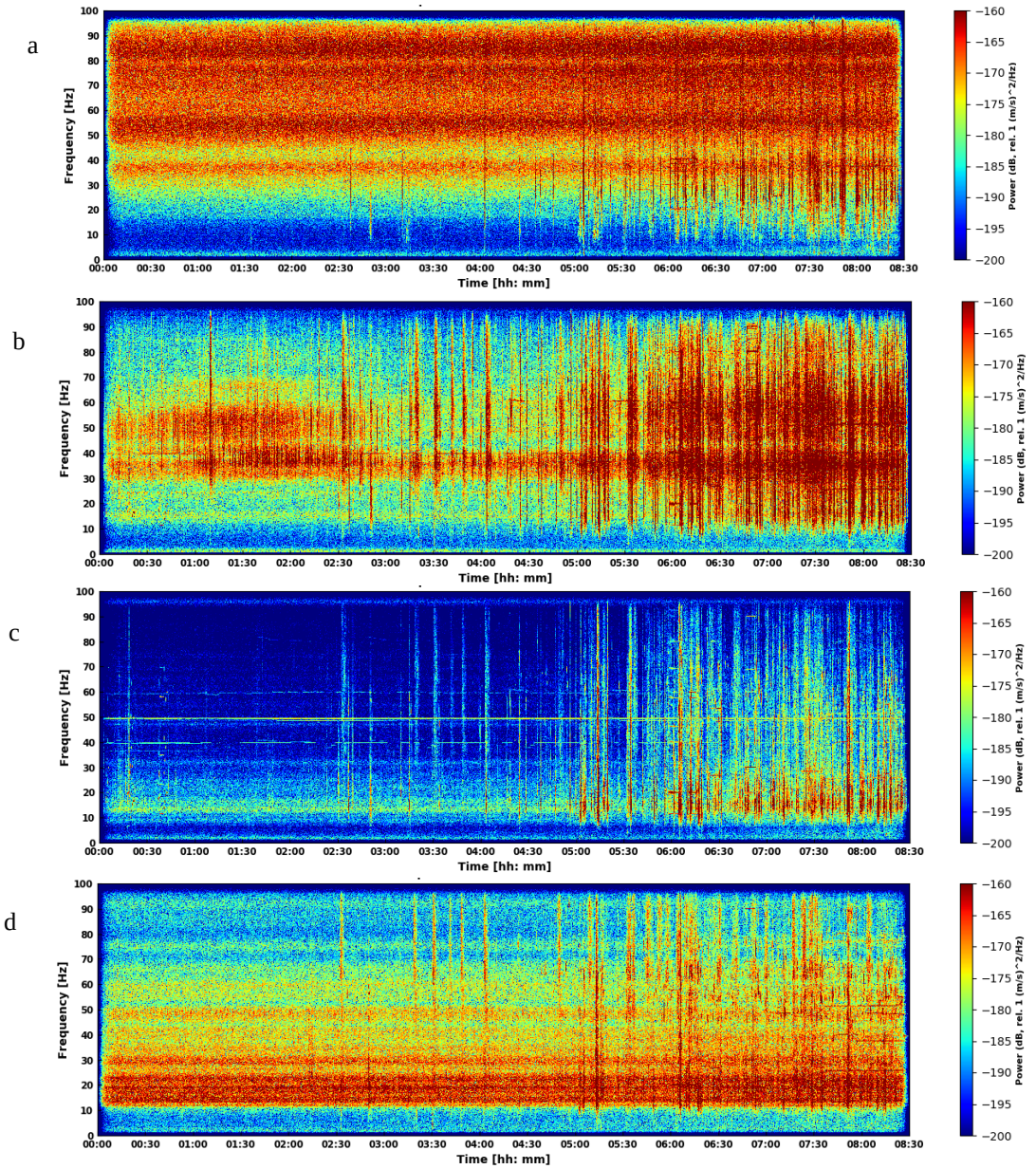

Figure 3. (a-d): The spectrogram of stations AV002, AV009, AV003, and AV011 on October 15th 2019, respectively. The frequency content of the tremor depends on the station's distance to the river. The noise-induced by cultural activity appears as vertical spikes on the spectrograms. The cultural noise boost from 5:00 A.M. which is the start of daily human activities.

Figures S1-S5 in supplementary material demonstrate the result of beamforming for each discrete frequency band mentioned above. We noticed the tremor has a spectral signature in the frequency range 8-17 Hz as shown in Figure 4. The change in wave speed after 5:00 A.M. reflects the start

of the daily human activities. In this case, the cultural noise has a similar BAZ as the river. Therefore, there are two possibilities: either the cultural noise is coming from the same direction as the river or the cultural noise is amplified and trapped within the river. This is a hypothesis which needs further investigation. The persistent frequency in the range of 17-19 and 19-22 Hz are not river-induced. Note in Figures S4 and S5, the BAZ of the persistent non-river induced signal is different to the cultural noise that kicks in after 5:00 A.M.

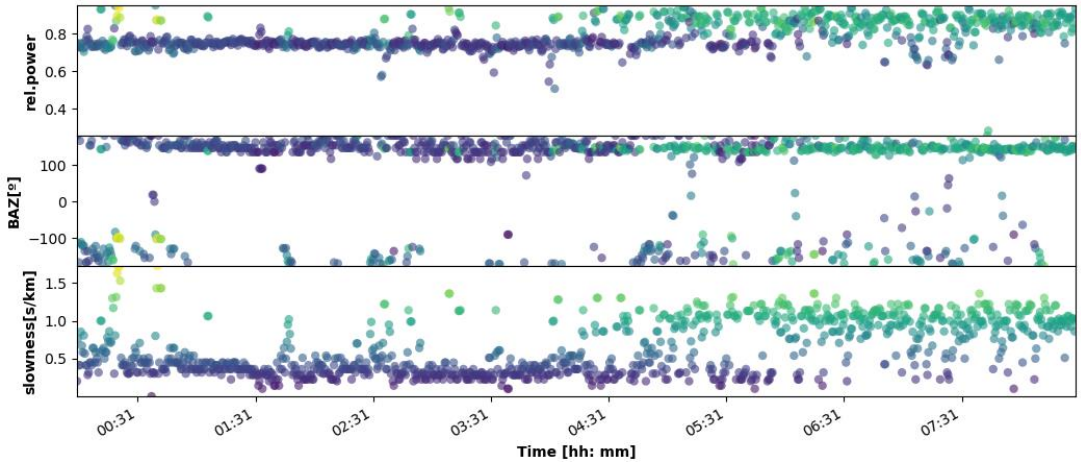

Figure 4. Beamforming array-processing results for the first array in the frequency range 8-17 Hz From top to bottom the time-series indicate relative power (semblance), BAZ, and slowness. All panels are colour-coded based on slowness. The tremor shows a persistent BAZ as expected. Sudden changes in BAZ occur at a time of strong cultural noise. Note the change in wave speed after 5:00 A.M. when daily human activities start. This is also reflected in the enhanced relative power after 5:00 A.M.

We bandpass filtered the seismic data in the discrete frequency bands observed as persistent on the spectrograms of the second array including 10-14.65, 13-17, 21-23, 30-32 and 32-36 Hz, and applied the FK analysis similar to the first array. Figures S6-S12 in the supplementary material demonstrate the results of beamforming for each discrete frequency band mentioned above. We noticed that the tremor has a spectral signature in the frequency range 10-23 Hz as shown in Figure 5. The persistent frequency in the range 23-27, 27-30, 30-32 and 32-36 Hz are not river-induced as shown in Figures S6 to S12. Note that we do not observe any change in the slowness of the tremor after 5:00 A.M. for the second array compared to the first array. Our interpretation is that the second array is more distant to the source of the cultural noise compared to the first array.

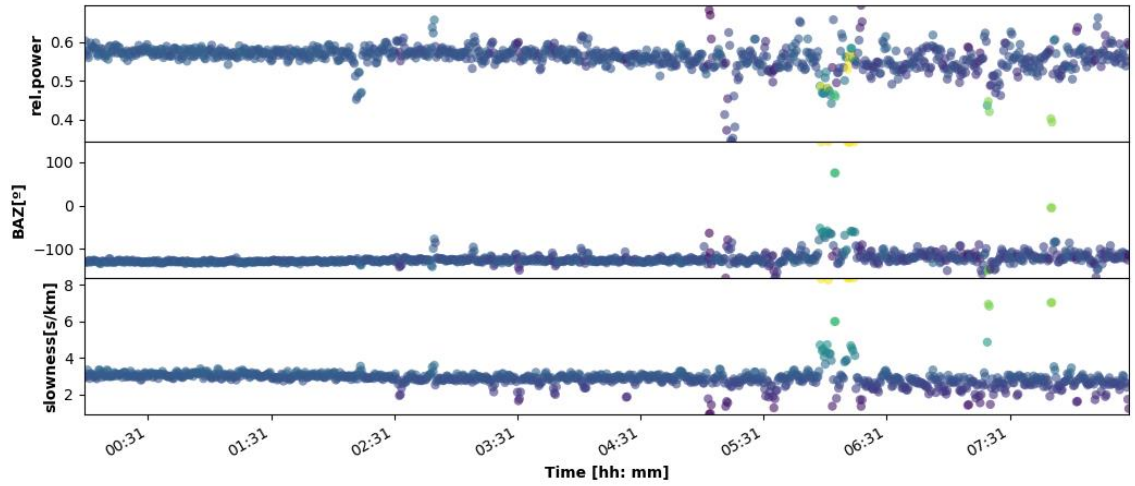

Figure 5. Beamforming array-processing results for the second array in the frequency range 10-23 Hz. From top to bottom the time-series indicate semblance, absolute power, BAZ, and slowness. All panels are colour-coded based on slowness. The tremor shows a persistent BAZ as expected.

Figure 6 shows the application of beamforming to the whole dataset between October 10th – October 15th 2019 with 20 minutes window length of 50% overlap. Note that due to averaging, the effect of cultural noise is eliminated and the tremor shows up as persistent BAZ and slowness.

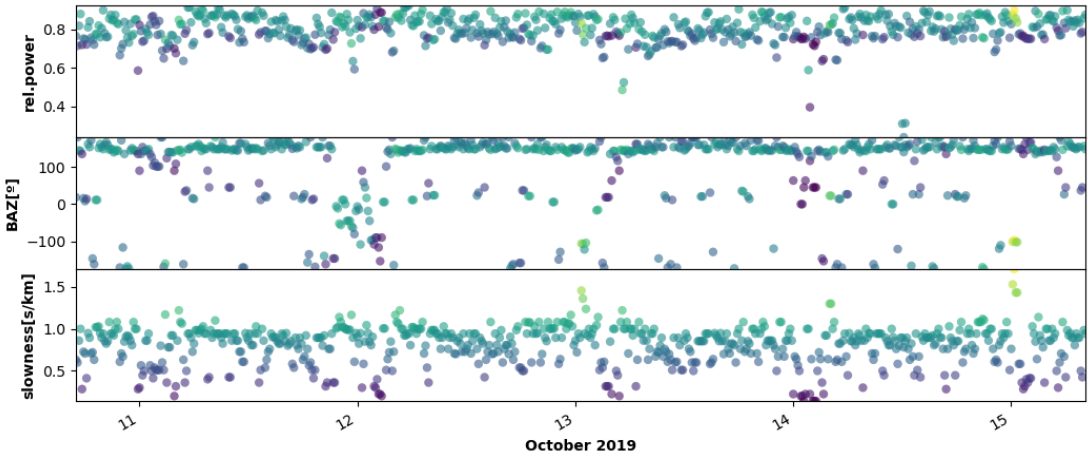

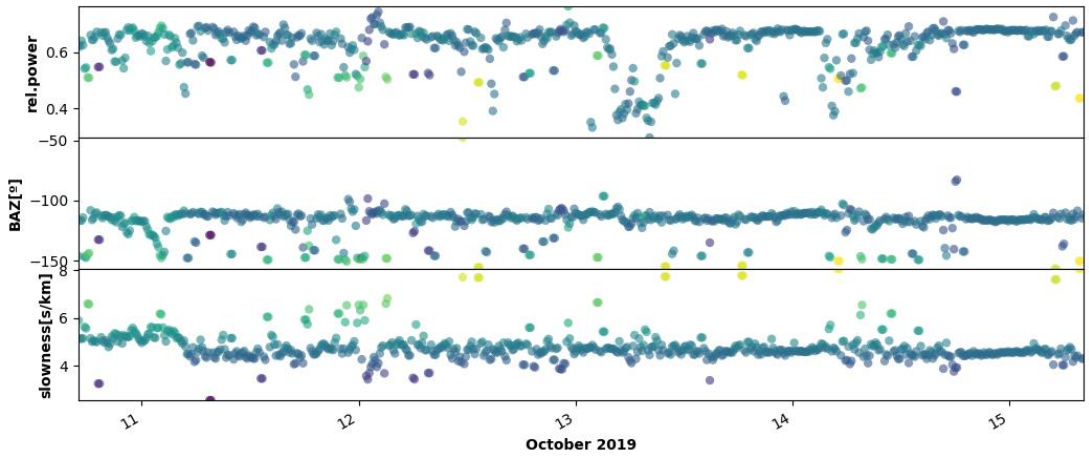

Figure 6. Beamforming array-processing results for the (top): first and (bottom): second array in the frequency range 8-17 and 10-23 Hz, respectively for the whole data recording interval between 10^{th}-15^{th} October 2019. The window length of 20 minutes with 50% overlap is used for FK analysis. Note the effect of cultural noise is eliminated due to longer window length and we observe a persistent BAZ and slowness for the river-induced signal. However, we still see change in BAZ and slowness during intervals of severe cultural noise.

Two or more arrays are usually used to find the epicentral location of the source. We note the BAZs of the two arrays in our study do not coincide at a common point. Since seismic records at one station are sensitive to a broad portion of the river near it (Burtin et al., 2008) the array analysis tends to detect the strongest 'point source' closest to the array, while the river can be considered as a spatial series of many point sources of varying strength,each array locates the strongest source, i.e., the strongest local point in the river, closest to it. Figure 7 depicts the BAZ of the tremor in the frequency range of 8-17 and 10-23 HZ for the first and second array, respectively.

Figure 7. Determining the direction of arrival of the tremor to each array by calculating the BAZ based on beamforming. Each array locates the strongest closest point source. The yellow icons show the stations in each array and the red lines depict the BAZ, i.e., the direction of arrival of

tremor in the frequency range of 8-17 and 10-23 Hz for the first and second array, respectively.

To further determine the wave composition of the tremor, we applied FDPA to data for the time interval between midnight to 5:00 A.M. and 5:00 A.M. to 8:30 A.M. as shown in Figures S13 and S14 in the supplementary material. The ratio between the first and second singular values of the spectral covariance matrix being above 2.5 was used to determine whether the signal is polarized or not. The wave type at each frequency is determined by applying a 20% threshold. To differentiate between body and Love waves, we looked at the power spectra of different components computed using the Welch method (Figure S15). When the horizontal powers are higher than the vertical one, the tremor is Love wave dominated. Figure 8 shows the wave percentage for these two time intervals for station AV003 as the representative element of the first array. Note that the highest percentage of the tremor is mixed waves at each frequency component. For the frequency range of 8-10 Hz Love waves dominate the remaining composition of the tremor for both of these time intervals. We did not observe any change in the slowness values of the tremor in these two time intervals for the frequency range 8-10 Hz (Figure S1). For the frequency range of 10-14 Hz, the tremor is Love wave dominated in the time interval midnight to 5:00 A.M while Rayleigh waves dominates in the interval 5:00 to 8:30 A.M. reflecting the beginning of human activities. This is consistent with the increase in the slowness values from array processing.

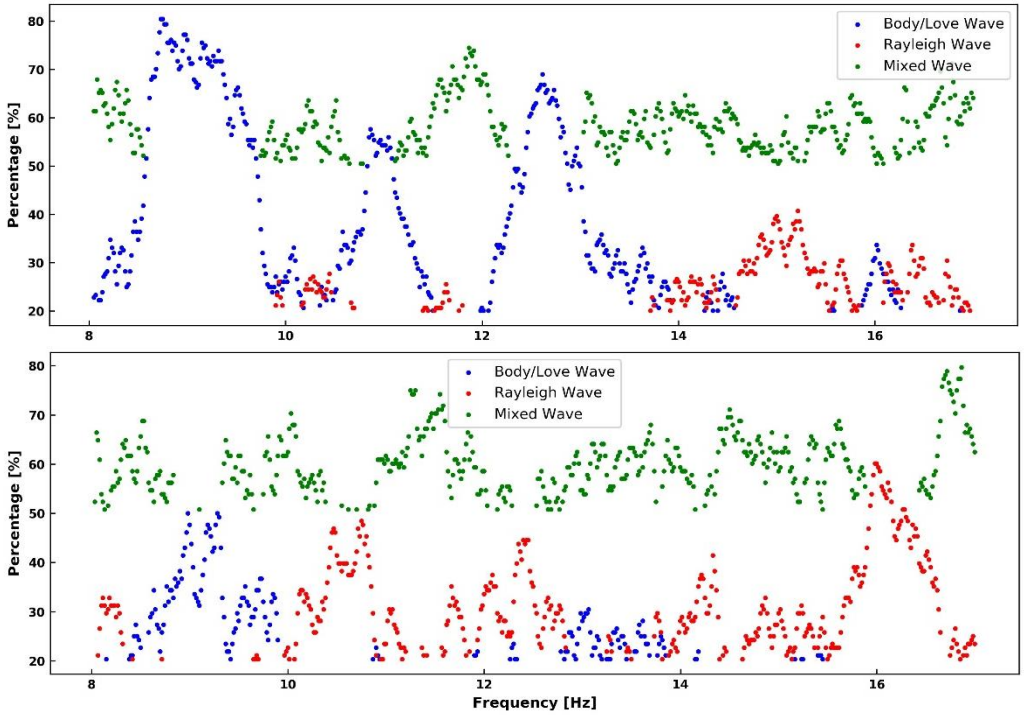

Figure 8. The percentage of different wave types in the tremor in the frequency range 8-17 Hz for station AV003 as the representative of the first array. For the time interval (top) midnight to 5:00 A.M. and (bottom) 5:00 to 8:30 A.M. on October 15th 2019. Note the tremor is mainly composed of mixed waves after which Love waves dominate. Note the enhancement of Rayleigh wave composition of the tremor once the cultural noise kicks in.

Figure 9 shows the wave percentage for these two time intervals for station AV011 as the

representative of the second array. Note the tremor contains mainly of Love waves. Moreover, the wave composition is similar for these two time intervals. This is consistent with the similar slowness values we obtained from array processing in these two time intervals.

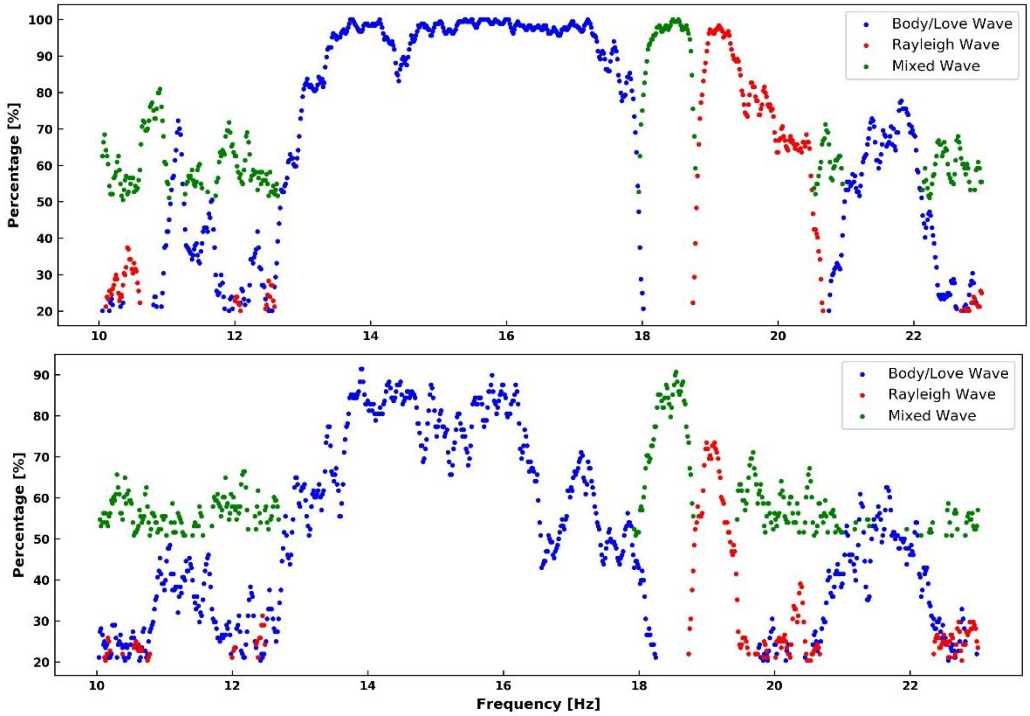

Figure 9. The percentage of different wave types in the tremor in the frequency range 10-23 Hz for station AV011 as the representative of the second array. For the time interval (top) midnight to 5:00 A.M. and (bottom) 5:00 to 8:30 A.M. on October 15th 2019. Note the tremor does not change in wave component in these two time intervals.

As stated by Vore et al. (2019) to locate the tremor in a particular frequency range, three criteria need to be met. First, the power spectrum should show a peak in that frequency range. This is where we observed the persistent signals on the spectrograms in Figure 3. Second, the signal should be polarized, i.e., well-constrained particle motion and third is that Rayleigh waves dominate. The BAZ, computed based on the Rayleigh components of the tremor, for station AV003 and AV013 as the representatives of the first and second array is 150º and 235º, respectively. This is in agreement with the BAZ of 160º and 240º derived from array processing for these arrays. This shows FDPA using a single 3C seismic station is a promising tool in the absence of seismic arrays to both locate tremors dominated by Rayleigh waves.

In the next step, we investigated the existence of correlation between the flow-rate recorded by the EPA flow-gauge and the seismic monitoring station, AV009, over the one and half months of deployment. Movie S1 in the supplementary material shows the spectrogram of the monitoring station AV009 between 10th October- 18th December 2019. Note the extent of cultural noise in the data. We computed median filtered spectrograms as proposed by Bartholomaus et al. (2015) to alleviate the effect of cultural noise on tremor amplitude. We then extracted the persistent signal in the frequency band between 11-14 Hz on the median-filtered spectrograms of the seismic

monitoring station. The root mean square of the sum of signal at each time sample in this frequency range yields a time series that we call Tremor as shown in Figure 10. Note there is reasonably good correlation between the Tremor and flow-rate except for the time intervals with extensive cultural noise due to the construction site operating near the monitoring station.

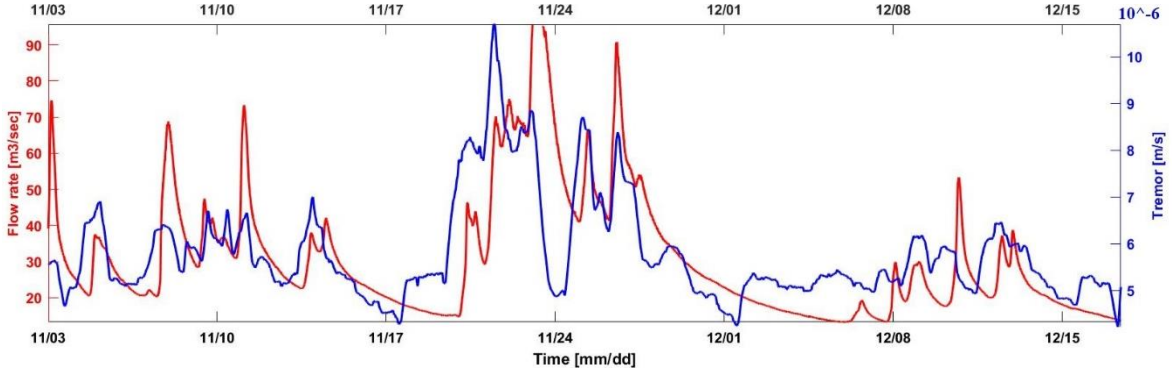

Figure 10. The correlation between the flow-rate and seismic tremor in the frequency range 11-14 Hz at the seismic monitoring station, AV009, Whitebridge, Co. Wicklow, Ireland between 10th October- 18th December 2019. This confirms the capability of fluvial seismology as hydrological monitoring tool for rivers even in the presence of strong cultural noise.

5 Conclusions

This study investigated the passive seismic approaches to locate and characterize the seismic tremor induced by Avoca river, Co. Wicklow, Ireland. As this river located near a construction site and a busy local road and residential area, it was necessary to differentiate the river-induced signal to be called tremor from the cultural noise. We used beamforming array processing to locate the tremor in discrete frequency bands observed persistent on spectrograms. We could locate the persistent 8-17 Hz tremor on the first (upstream) and 10-23 Hz tremor on the second (downstream) array. The wave speed changes for the stations in the first array after 5:00 A.M. which is the start of the daily human activity. This observation was in accordance with the dominance of Rayleigh wave components in the tremor on the stations after 5:00 A.M. based on FDPA. When Rayleigh waves dominated the tremor, we could determine the direction of arrival based on the slope of the amplitude ratio between the horizontal components which gave consistent results compared to the BAZ calculated from the array processing. This shows FDPA using a single 3C seismic station is a promising tool in the absence of seismic arrays. Finally, the correlation between flow-rate and the tremor power computed based on the root square of the median filtered spectrograms integrated within the frequency range of the tremor on the monitoring seismic station confirms the capability of fluvial seismology to constraint hydrological properties of rivers even in the presence of strong cultural noise.

Acknowledgments

We used the freely available software Obspy (Megies et al., 2011) for pre-processing seismic data and beamforming array analysis. We used MatLab for producing the median filtered spectrograms. We used the freely available code (Vore et al., 2019) for performing FDPA. We used the freely available software Geopsy (Wathelet et al., 2020) for analyzing HVSR. This project is part of the Geohazard spoke of the Irish Center for Research in Applied Geosciences (iCRAG) funded by the Science Foundation of Ireland (SFI). We acknowledge the Geological Survey Ireland (GSI) and

Transport Infrastructure Ireland (TII) for financially supporting this project. We thank the Wicklow County Council for providing the site access to deploy seismic stations near Avoca River. We are highly grateful to Dr. David Craig, the field technician at DIAS for his great assistance during the fieldwork.

Open Research

The raw seismic data used in this study can be obtained by contacting the Dublin Institute for Advanced Studies (DIAS). The water-level and flow-rate data can be freely downloaded from the Environmental protection Agency (EPA) (https://epawebapp.epa.ie/hydronet). The corresponding author of the paper can be contacted to access the codes used in this study.

References

Anthony, R.E., Aster, R.C., Ryan, S., Rathburn, S., Baker, M.G., 2018, Measuring Mountain River Discharge Using Seismographs Emplaced Within the Hyporheic Zone, *Journal of Geophysical Research: Earth Surface*, 123, 1-19.

Bartholomaus, T.C., Amundson, J.M., Walter, J.I., O'Neel, S., West, M.E., Larsen, C.F., 2015, Subglacial discharge at tidewater glaciers revealed by seismic tremor, *Geophys. Res. Lett.*, 42, 6391–6398.

Burtin, A., Bollinger, L., Vergne, J., Cattin, R., Nabelek, J.L., 2008, Spectral analysis of seismic noise induced by rivers: a new tool to monitor spatiotemporal changes in stream hydrodynamics, *J. Geophys. Res*. 113 (B5) B05301.

Burtin, A., Vergne, L.B.J., Cattin, R., Nabelek, J., 2011, Towards the hydrologic and bed load monitoring from high-frequency seismic noise in a braided river: the 'torrent de st pierre', French Alps, *J. Hydrol*, 408 (1-2), 43–53.

Eibl, E.P.S., Bean, C.J., Einarsson, B., Palsson, F., Vogfjord, K.S., 2020, Seismic ground vibrations give advanced early-warning of subglacial floods, *Nature Communications*, 2504, 1-11.

Gimbert, F., Tsai, V.C., Lamb, M.P., 2014, A physical model for seismic noise generation by turbulent flow in rivers, *J. Geophys. Res. Earth Surf*, **119**, 2209–2238.

Goodling, P.J., Lekic, V., Prestegaard, K. 2018, Seismic signature of turbulence during the 2017 Oroville Dam spillway erosion crisis, *Earth Surf. Dynam.*, 6, 351–367.

Govi, M., Maraga, F., Moia, F., 1993, Seismic detectors for continuous bed load monitoring in a gravel stream, *Hydrol. Sci. J.*, 38, 123–132.

Hsu, L., Finnegan, N.J., Brodsky, E.E., 2011. A seismic signature of river bedload transport during storm events, *Geophysical Research Letter*, 38 (13), L13407.

Larose E., 2015, Environmental seismology: What can we learn on earth surface processes with ambient noise?, 2015, *Journal of Applied Geophysics*, 116, 62- 74.

Megies, T., Beyreuther, M., Barsch, R., Krischer, L. &Wassermann, J., 2011, ObsPywhat can it do for data centers and observatories?, *Ann. Geophys*., 54, 4758.

Park, J., Vernon, F.L, Lindberg, C.R., 1987, Frequency Dependent Polarization Analysis of High-Frequency Seismograms, *Journal of Geophysical Research*, 92(B12), 12664-12674.

Roth, D.L., Finnegan, N.J., Brodsky, Rickenmann, D., Turowski, J.M., Badoux, A., Gimbert, F., 2017, Bed load transport and boundary roughness changes as competing causes of hysteresis in the relationship between river discharge and seismic amplitude recorded near a steep mountain stream, *J. Geophys. Res. Earth Surf.*, 122, 1182- 1200.

Schmandt, B., Aster, R.C., Scherler, D., Tsai, V.C., Karlstrom, K.K., 2013, Multiple fluvial processes detected by riverside seismic and infrasound monitoring of a controlled flood in the Grand Canyon, *Geophys. Res. Lett*, 40, 4858–4863.

Schmandt, B., Gaeuman, D., Stewart, R., Hansen, S.M., Tsai, V.C., Smith, J., 2017, Seismic array constraints on reach-scale bedload transport, *Geology*, 45(4), 299-302.

Tsai, V.C., Minchew, B., Lamb, M.P., Ampuero, J.-P., 2012, A physical model for seismic noise generation from sediment transport in rivers, *Geophysical Research Letters*, 39, L02404.

Vore, M.E., Bartholomaus T.C., Winberry J.P., Walter J.I. and Amundson J.M., 2019, Seismic Tremor Reveals Spatial Organization and Temporal Changes of Subglacial Water System, *Journal of Geophysical Research*, 124, 427- 446.

Wathelet, M., Chatelain, J.-L., Cornou, C., Di Giulio, G., Guillier, B., Ohrnberger, M. and Savvaidis, A., 2020, Geopsy: A User-Friendly Open-Source Tool Set for Ambient Vibration Processing, *Seismological Research Letters*, 91(3), 1878- 1889.

Winberry, J.P., Anandakrishnan, S. and Alley, R.B., 2009, Seismic observations of transient subglacial water-flow beneath MacAyeal Ice Stream, West Antarctica, *Geophysical Research Letter*, 36, L11502.